Analysis of bond-loss resistance models for pretensioned I-girders

Behnam Naji, Brandon E. Ross, and Amin Khademi

- Bond-loss failure is associated with shear cracking near the support that interrupts anchorage of the strands, leading to loss of bond and slipping of the strands relative to the concrete.
- This paper presents a database of bond-loss failures that are documented in the research literature and uses the database to create a bond-loss failure model.
- A key insight from the refined model is that stress in transverse reinforcement attendant with bond-loss failure is often less than yield stress.

The end region of a pretensioned girder must perform two critical functions: it must facilitate the transfer of forces from the prestressing strands to the concrete, and it must carry shear forces from the girder to the support. This paper focuses on the transfer of shear forces in the end region and aims to refine a previously proposed model for end-region bond-loss resistance.[1] The refined model is compared with the requirements in the American Association of State Highway and Transportation Officials' *AASHTO LRFD Bridge Design Specifications*[2] for proportioning flexural reinforcement in the end region. The comparison demonstrates that the refined model provides improved accuracy and conservatism relative to the AASHTO LRFD specifications.

Failures involving loss of strand-concrete bond have been observed in many load tests of precast, pretensioned concrete I-girders.[3,4] Bond-loss failure is characterized by the formation of cracks in the end region due to applied loads (**Fig. 1**). These cracks interrupt the anchorage of strands, leading to loss of bond and slipping of strands relative to the concrete[5] (Fig. 1). Strand slip allows the crack to open wider and causes rotation about the crack tip. Once the slip and resulting rotation are sufficient, the beam will fail as the compression zone crushes under a combination of shear and flexural actions. The specifics of bond-loss behavior can vary from specimen to specimen; the terminology and mechanics associated with different types of bond-loss failures are described in detail by Naji et al.[6]

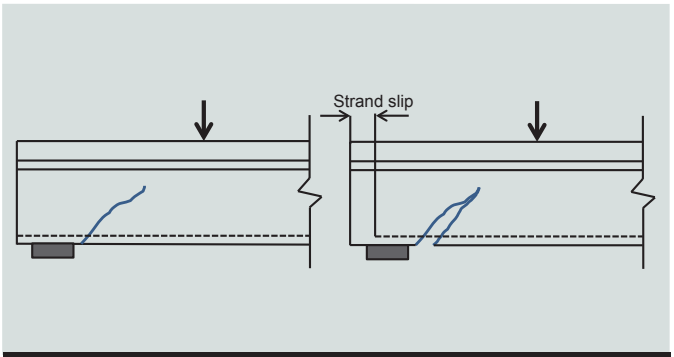

Figure 1. Basic description of bond-loss failure: crack forms near support (left) and crack leads to bond loss and strand slip (right).

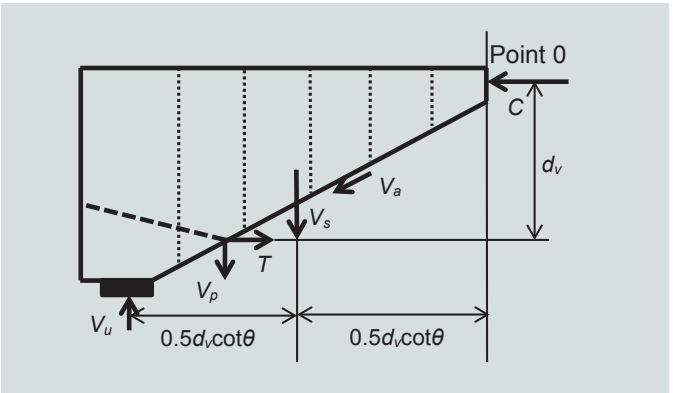

Figure 2. Free body diagram of end region (based on 2014 *AASHTO LRFD Bridge Design Specifications*). Note: C = force in compression zone; d_v = effective shear depth; T = longitudinal tie force in flexural reinforcement; V_a = force along crack interface; V_p = component of prestressing in direction of the shear force; V_s = resistance provided by the vertical reinforcement; V_u = factored shear force; θ = angle of inclination of diagonal compressive stresses.

It has been experimentally observed that failure due to loss of strand-concrete bond can lead to capacities that are less than nominal shear and nominal flexural strength.[4,7] Because bond loss can be the controlling factor in capacity,[8,9] it is critical that bond-loss resistance be considered when designing I-girder end regions. Toward the goal of understanding and designing for this failure mode, the first part of this paper presents a database consisting of 120 specimens that had bond-loss failure. This database provides a means of exploring the mechanisms and variables that contribute to bond-loss failures. The second part of this paper presents a refined model for calculating the nominal bond-loss resistance of pretensioned I-girders. Quantitative methods, including the least squares method and linear regression, were used in developing the model. The database and model presented in this paper are expanded and refined from the authors' previous work.[1] The third and final part of this paper includes example calculations to demonstrate the bond-loss resistance model. It is intended that the database, refined model, and example calculation contribute to the design of safe and efficient precast, pretensioned concrete I-girders. The refined model is more accurate than the AASHTO LRFD specifications because it corrects some potentially unconservative scenarios.

Background

AASHTO LRFD specifications

Although bond-loss resistance is not specifically mentioned in the AASHTO LRFD specifications, the concept is implicitly addressed in Eq. 5.8.3.5-2 (Eq. [1]). This equation is used for proportioning flexural reinforcement to carry longitudinal tie forces at the inside edge of simple-span supports. This equation is based on the equilibrium of the end region and can be derived through the summation of moments about point 0 (**Fig. 2**). The end region considered by the AASHTO LRFD specifications (Fig. 2) is similar to the girder portion that is adjacent to the support in a bond-loss failure (Fig. 1). In both cases a crack separates the end region from the remainder of the girder.

$$A_s f_y + A_{ps} f_{ps} \geq \left(\frac{V_u}{\phi_v} - 0.5V_s - V_p \right) \cot\theta \qquad (1)$$

where

A_s = area of nonprestressing tension steel

f_y = specified yield strength of reinforcement bars

A_{ps} = area of prestressing steel

f_{ps} = average stress in prestressing steel coincident with V_u

V_u = factored shear force

ϕ_v = resistance factor for shear

V_s = resistance provided by the vertical reinforcement

V_p = component of prestressing in direction of the shear force

θ = angle of inclination of diagonal compressive stresses

The intent of the provision in the AASHTO LRFD specifications is to ensure that sufficient transverse and longitudinal reinforcement are present to maintain equilibrium in the end region. Bond-loss failure is implicitly addressed in section 5.8.3.5, which requires that "any lack of full development length [of the longitudinal tie] shall be accounted for" when using Eq. (1). However, explicit requirements are not given for how to account for a lack of full development. In lieu of explicit requirements, multiple authors[1,8,9]

have suggested that a reduced strand capacity can be calculated based on the strand embedment length between the end of the girder and the assumed inclined cracks. The transfer length provisions of the AASHTO LRFD specifications section 5.11.4 are used by these authors to calculate the reduced strand capacity.

Assuming that bond loss of the flexural reinforcement controls end-region capacity, Eq. (1) can be rearranged into Eq. (2) to calculate nominal bond-loss capacity. This approach has been used by multiple authors[7,8] to modify the AASHTO LRFD specifications equation for calculating bond-loss capacity.

$$\frac{V_u}{\phi_v} \le V_{nb} = \frac{A_s f_y + A_{ps} f_{psb}}{\cot\theta} + 0.5V_s + V_p \qquad (2)$$

where

V_{nb} = nominal bond capacity

f_{psb} = stress in prestressing strand coincident with bond-loss failure

Original bond-loss model

Ross and Naji[1] previously proposed a model for calculating nominal capacity of a pretensioned I-girder end region against bond-loss failure and compared the model with a database of 84 experimental tests. The previously proposed model is referred to as the *original model*. Similar to the provisions of the AASHTO LRFD specifications section 5.8.3.5, the original model (**Fig. 3**) is based on moment equilibrium of the end region; however, the model relies on fewer simplifications and is consequently applicable to a wider range of girders.

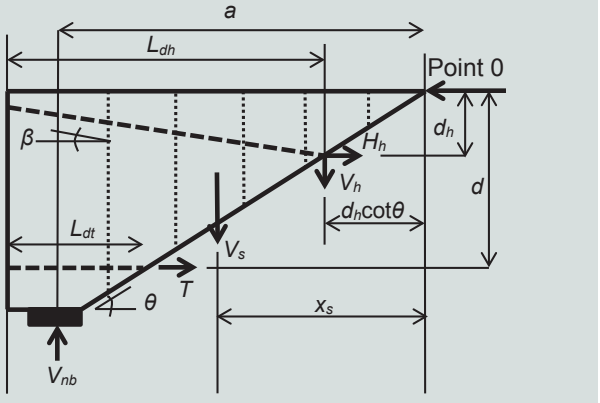

Figure 3. Free body diagram of end region for original model. Note: a = shear span; d = flexural depth of tension tie; d_h = depth of harped strands at crack interface; H_h = horizontal force in harped strand; L_{dh} = available embedment length of harped strand; L_{dt} = available embedment length of tension tie; T = longitudinal tie force in flexural reinforcement; V_h = vertical force in harped strand; V_{nb} = nominal bond capacity; V_s = resistance provided by the vertical reinforcement; x_s = horizontal distance to vertical steel centroid; β = inclination angle of harped strands; θ = angle of inclination of diagonal compressive stresses.

Key differences between the original model (Fig. 3) and the free body diagram used in the AASHTO LRFD specifications (Fig. 2) include the following:

- Harped strands are treated separately from the straight strands.
- Nonuniformly distributed reinforcement is considered by locating the resultant force from vertical reinforcement at a variable location x_s.
- Available development length of the tension tie and harped strands are explicitly considered by introducing variables L_{dt} and L_{dh}, respectively.
- Flexural depth d is used in lieu of the effective shear depth d_v.

Equation (3) for nominal bond-loss resistance can be derived by summing moments about point 0 in Fig. 3:

$$V_{nb} = \frac{V_s x_s}{d\cot\theta} + \frac{T}{\cot\theta} + \frac{V_h d_h}{d} + \frac{H_h d_h}{d\cot\theta} \qquad (3)$$

where

x_s = horizontal distance to vertical steel centroid

T = longitudinal tie force in flexural reinforcement

V_h = vertical force in harped strand

d_h = depth of harped strands at crack interface

H_h = horizontal force in harped strand

When applying Eq. (3) to analyze test specimens, shear span–to–depth ratio a/d is assumed to equal cot θ. This is based on the observation that inclined cracks in tests are often oriented along a line between the support and load point.[1]

The longitudinal tie force T is calculated as Eq. (4).

$$T = A_s f_y + A_{ps} f_{pe}\left(\frac{L_{dt}}{L_t}\right) \qquad (4)$$

where

f_{pe} = effective stress in prestressing steel

L_t = required transfer length

The area of prestressing only includes fully bonded straight strands. Debonded strands cannot contribute to the tension tie and bond-loss resistance.

Equation (5) calculates the resistance provided by the vertical reinforcement.

$$V_s = A_v f_y \quad (5)$$

where

A_v = area of vertical reinforcement crossing assumed crack plane

Equation (4) follows the same approach as the AASHTO LRFD specifications section 5.11.4. The force in the strands is calculated as being linearly proportional to the available length of embedment L_{dt}. The maximum possible force in the strands is taken as the effective prestress force, which occurs at the transfer length L_t. When harped strands are present, the same approach is used to calculate forces V_h and H_h, but with a different available development length L_{dh}. In this manner, the original model addresses the requirement of the AASHTO LRFD specifications section 5.8.3.5 to account for the lack of full development length.

One key insight from the development of the original model is that transverse reinforcement does not necessarily yield before or during bond-loss failure. The original model uses Eq. (6) to account for this circumstance. The equation is used to calculate stress in transverse reinforcement that is attendant at bond-loss failure. Equation (6) was constructed empirically, and factors f_1, f_2, and κ_{sv} were selected using a guess-and-check approach to fit the original model with the 84 specimens in the bond-loss database.

$$f_{sv} = (f_1 - f_2 \cot\theta)(1 - \kappa_{sv}\rho_{sv}) \le f_y \quad (6)$$

where

f_{sv} = stress in vertical reinforcement

f_1 = empirical factor taken as 130 ksi (900 MPa)

f_2 = empirical factor taken as 28 ksi (190 MPa)

κ_{sv} = empirical factor taken as 26

ρ_{sv} = shear reinforcement ratio

In Eq. (6), the shear reinforcement ratio is calculated as Eq. (7).

$$\rho_{sv} = \frac{A_v}{b_w d \cot\theta} \quad (7)$$

where

b_w = web width

The current study improves on the original study by expanding and refining the database and by using statistical linear regression analysis and the least squares method to identify best-fit equations with the experimental data.

Expanded bond-loss database

The original bond-loss database included 84 specimens from 10 different sources.[3,4,7,10–16] In the current study, 44 specimens from 11 different test programs[5,8,17–25] were added. In addition, 8 specimens from Barnes et al.[13] were removed because they only experienced bond loss and strand slip in shielded (partially debonded) strands. Thus, all specimens in the expanded database (**Table 1–3**) experienced strand slip in fully bonded strands and failed according to the mechanics and models described in the previous sections. Tables 1 through 3 also report the nominal bond capacity from the refined model, which is discussed later in this paper.

Specimens in the expanded database cover a range of variables. Tested compressive strength of concrete was typically reported in the reference and was used to calculate bond-loss capacity. Approximately half of the specimens had concrete with tested compressive strength greater than 7200 psi (50 MPa) at the time of load testing. All database specimens had 270 ksi (1860 MPa) ultimate strength strands. Nine of the specimens had both harped and straight strands. The remaining 111 specimens had only straight strands. The specified yield strength of the mild reinforcement was 60 ksi (410 MPa) in 114 of the specimens and 40 ksi (280 MPa) in the remaining 6. All specimens in the database were simply supported and were load tested at a/d ranging from 1.0 to 4.4.

Development of refined bond-loss model

The expanded bond-loss database, including 120 specimens, was used to calculate the bond-loss capacity given by Eq. (3) through (5). **Figure 4** presents the results according to the strength ratio V_{nb}/V_{exp}, where V_{exp} is the experimental capacity. The figure shows the strength ratio of each database specimen plotted against six different variables. A strength ratio greater than one indicates that the calculated result is unconservative (larger) relative to the experimental result. Equations (3) through (5) in their current form are not an accurate representation of bond-loss capacity of pretensioned I-girders (Fig. 4). Using these equations for design can result in understrength members. If the model were ideal, all the points would fall at a strength ratio of 1.0; however, the calculated strength ratios

Table 1. List of specimens 1 through 41

Specimen number	Reference	Specimen ID	V_{nb}	V_{exp}	V_{nb}/V_{exp}
1	7	G1	291.9	344.0	0.848
2		G2	211.9	255.0	0.831
3		G3	171.7	207.0	0.829
4		G4-2	147.5	198.0	0.745
5	11	B5M-C	130.4	162.0	0.805
6		B5L-C	144.9	179.0	0.809
7		B6S-C	122.1	165.0	0.740
8		B6M-C	131.3	180.0	0.730
9		B6L-C	148.4	188.0	0.789
10	16	PS1-0	27.7	27.2	1.018
11		PS2-S6M	30.5	34.0	0.898
12		PS3-D2	33.9	35.1	0.965
13		PS4-M2	30.7	32.9	0.935
14		PS5-0	27.7	25.7	1.080
15		PS6-WD	29.9	31.3	0.955
16		PS7-WSH	30.4	30.2	1.007
17		PS8-WS	30.4	27.7	1.100
18		PS9-WDH	30.0	28.8	1.043
19	12	I-3	63.4	100.0	0.634
20		I-4	56.4	110.0	0.513
21		II-1	89.3	140.0	0.638
22	4	A0-00-R-N	193.2	313.0	0.617
23		A1-00-M-N	123.7	141.0	0.877
24		A1-00-M-S	137.7	168.0	0.819
25		A1-00-R/2-N	141.7	166.0	0.853
26		A1-00-R/2-S	138.9	173.0	0.803
27		A1-00-R-N	177.6	210.0	0.846
28		A1-00-3R/2-N	213.5	207.0	1.031
29		B0-00-R-N	175.9	220.0	0.799
30		B0-00-2R-N	247.7	223.0	1.111
31		B0-00-3R-N	319.6	231.0	1.383
32		B1-00-0R-N	156.1	166.0	0.940
33		B1-00-0R-S	152.1	155.0	0.981
34		B1-00-R-N	223.2	245.0	0.911
35		B1-00-R-S	219.9	232.0	0.948
36		B1-00-2R-N	290.4	262.0	1.108
37		B1-00-2R-S	287.8	247.0	1.165
38		B1-00-3R-N	355.7	264.0	1.347
39		B1-00-3R-S	355.6	263.0	1.352
40		B1-00-2R2-N	289.1	268.0	1.079
41		B1-00-2R2-S	287.8	255.0	1.129

Note: V_{exp} = experimental bond capacity; V_{nb} = nominal bond capacity from the refined model.

Table 2. List of specimens 42 through 83

Specimen number	Reference	Specimen ID	V_{nb}	V_{exp}	V_{nb}/V_{exp}
42	3	5-1-EXT	95.8	91.2	1.050
43		5-1-INT	97.9	107.0	0.915
44		5-2-EXT	111.0	104.0	1.067
45		5-2-INT	110.5	98.1	1.127
46		5-3-INT	112.2	115.0	0.976
47		5-4-INT	120.3	112.0	1.074
48		5-SWAI-WEST	98.0	125.0	0.784
49		5-UWR-EAST	101.9	115.0	0.886
50		5-UWR-WEST	102.8	134.0	0.767
51		5-FWC-EAST	95.3	117.0	0.815
52		5S-1-EXT	118.3	109.0	1.085
53		5S-1-INT	116.8	117.0	0.998
54		5S-2-INT	118.5	100.0	1.185
55		5S-3-EXT	103.8	103.0	1.008
56		5S-3-INT	104.4	103.0	1.014
57		5S-4-EXT	107.4	112.0	0.959
58		5S-4-INT	106.9	122.0	0.876
59		916-1-EXT	98.7	83.9	1.176
60		916-1-INT	101.0	105.0	0.962
61		916-2-EXT	104.5	90.0	1.162
62		916-2-INT	105.3	102.0	1.033
63		916-3-EXT	95.3	90.1	1.057
64		916-4-EXT	95.5	82.9	1.152
65		6-2-EXT	87.9	103.0	0.854
66		6-2-INT	88.7	116.0	0.765
67		6-3-EXT	112.7	110.0	1.024
68	10	WN	503.8	534.0	0.944
69		WB	503.8	639.0	0.788
70		SL	582.6	609.0	0.957
71	14	G1E	453.0	572.0	0.792
72		G1W	631.5	662.0	0.954
73		G2E	680.0	743.0	0.915
74		G2W	892.5	852.0	1.048
75		G6W	548.0	612.0	0.895
76	15	AVW14608Y	285.0	460.0	0.620
77	13	L0B-B-72	210.8	175.6	1.200
78		L0B-D-54	238.4	236.2	1.009
79		L0B-C-54H	270.5	240.8	1.123
80		M0B-D-54	352.3	305.1	1.155
81		M0B-C-54H	384.0	314.3	1.222
82		H0B-D-54	394.8	308.8	1.278
83		H0B-C-54H	426.4	311.9	1.367

Note: V_{exp} = experimental bond capacity; V_{nb} = nominal bond capacity from the refined model.

Table 3. List of specimens 84 through 120

Specimen number	Reference	Specimen ID	V_{nb}	V_{exp}	V_{nb}/V_{exp}
84	21	G1A-E	340.8	362.8	0.939
85		G1B-E	224.6	312.2	0.719
86		G1C-E	209.9	289.2	0.726
87	20	G2BS	297.8	292.9	1.017
88		G4BS	363.3	328.9	1.105
89		G4AS	294.0	254.1	1.157
90	23	BT6-Live End	423.7	592.0	0.716
91		BT6-Dead End	419.5	557.0	0.753
92		BT7-Live End	608.1	614.0	0.990
93		BT7-Dead End	505.9	605.0	0.836
94	5	2B	134.5	110.9	1.214
95		2D	88.8	98.3	0.903
96		3B	134.5	91.4	1.472
97		3D	71.8	67.4	1.065
98	17	II-1A	154.1	222.0	0.694
99		I-3A	97.8	113.5	0.861
100	22	B4E2	353.9	387.7	0.913
101	18	SS2-SCCF2	195.4	222.9	0.876
102	25	F8N	184.8	180.0	1.026
103		F8S	195.0	222.0	0.878
104		F12N	222.9	216.0	1.032
105		F12S	233.0	275.0	0.847
106	19	3--1	65.5	63.2	1.036
107		3--2	65.5	65.2	1.004
108		3--3	39.3	41.0	0.958
109	24	R-8-North	198.1	277.0	0.715
110		R-8- South	208.3	302.0	0.690
111		2R-8-North	294.5	235.0	1.253
112		2R-8-South	304.4	256.0	1.189
113		R-10-South	232.3	299.0	0.777
114		2R-10-North	342.6	240.0	1.428
115		2R-10-South	352.5	245.0	1.439
116		R-12-North	246.3	279.0	0.883
117		R-12-South	256.4	276.0	0.929
118		2R-12-North	390.8	279.0	1.401
119		2R-12-South	400.5	287.0	1.396
120	8	Q-8	836.3	543.0	1.540

Note: V_{exp} = experimental bond capacity; V_{nb} = nominal bond capacity from the refined model.

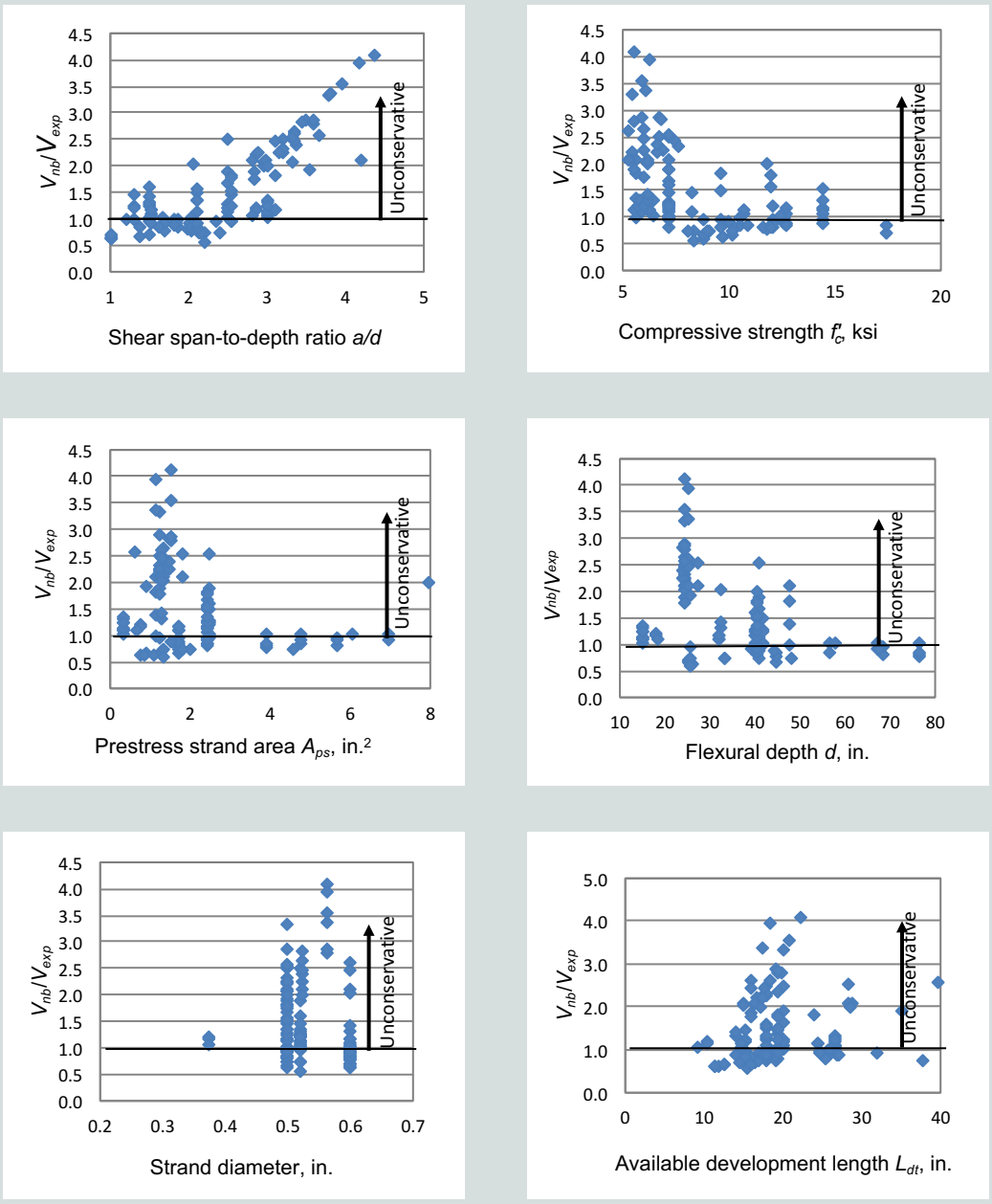

Figure 4. Strength ratios for original model compared with specimen parameters. Note: V_{exp} = experimental bond capacity; V_{nb} = nominal bond capacity. 1 in. = 25.4 mm; 1 ksi = 6.895 MPa.

Figure 4 shows an apparent trend between *a*/*d* and the strength ratio. For specimens with *a*/*d* less than 2.0, the strength ratios are typically near 1.0; however, as *a*/*d* increases, the strength ratios also increase and the model becomes more unconservative. The highest strength ratio is over 4.0 and corresponds to the largest *a*/*d*. Trends can also be observed for concrete compressive strength f'_c, flexural depth *d*, and prestress strand area A_{ps}. As these variables increase, the strength ratio decreases, which indicates a higher level of conservatism for these conditions.

The relationship between the nominal-to-experimental ratio and strand diameter and the available development length are not as obvious as the relationships observed for the other variables. To statistically identify whether the strength ratio has a significant correlation with the six independent variables, a linear regression model was developed for each variable.[26] This approach elucidates whether the value of the strength ratio changes when any one variable changes and the others are held fixed.

Table 4 shows the results of the regression analysis for each variable, where a low P value ($p < 0.05$) indicates that changes in a variable result in significant changes in the strength ratio. Conversely, a large P value suggests that changes in the variable do not result in significant changes

Table 4. Results of linear regression analysis

Variables	P value	Significant trend
Shear span–to–depth ratio a/d	7.26×10^{-25}	Yes
Concrete compressive strength f'_c	4.52×10^{-9}	Yes
Available embedment length of tension tie L_{dt}	0.254	No
Area of prestressing steel A_{ps}	0.004	Yes
Flexural depth of tension tie d	8.18×10^{-6}	Yes
Strand diameter	0.327	No

in the response. Results obtained from the regression analysis confirm observations made from Fig. 4 that changes in a/d, f'_c, d, and A_{ps} are related to changes in the strength ratio. Results also indicate that there is no clear trend between the strength ratio, length of embedment L_{dt}, and strand diameter.

While regression analyses are helpful for identifying important variables, it is also important to consider the physical phenomena that are underpinning the statistical results. Why is the accuracy of the model affected by these variables? The two most significant variables according to regression analysis are a/d and f'_c. The phenomena behind these observations are discussed in the following paragraphs. The trends observed for d and A_{ps}, while falling below the 0.05 P value threshold, are less significant than the trends of a/d and f'_c.

The effects of concrete compressive strength f'_c are considered first. Referring to Eq. (3), bond-loss capacity consists of four different terms. The first term is based on transverse reinforcement, and the remaining three terms are based primarily on contributions from prestressing strands. Recent research from Ramirez et al.[27] suggests that f'_c likely has an insignificant effect on the prestressing strand contribution of the database specimens. They found that transfer length, a critical parameter when calculating the contribution of the prestress strand to nominal bond capacity, is generally independent of concrete strength for f'_c greater than 5 ksi (34 MPa). All specimens in the database had a concrete compressive strength greater than 5 ksi, and it is reasoned that the observed trend with f'_c is not associated with the prestressing strand contribution to bond-loss capacity. This leaves the first term of Eq. (3) as the term affected by f'_c. The results presented in Fig. 4 and Table 4 assume yielding of the transverse reinforcement (f_{sv} equals f_y). This assumption is also made in the end-region provisions in AASHTO LRFD specifications section 5.8.3.5. The regression results suggest, however, that vertical reinforcement stress attendant with bond-loss failure is often less than yielding. Recalling that peak load of bond-loss failures is often based on failure of the compression zone,[6] it is reasoned that as f'_c decreases, strength of the compression zone decreases and peak capacity of the bond-loss mechanism occurs at lower loads. Because lower f'_c leads to reduced bond-loss capacity, attendant stress in the transverse reinforcement is limited by the concrete strength; that is, the concrete compression zone fails while the transverse reinforcement stress is less than the yield. Hence, transverse reinforcement stress at ultimate load was likely less than the yield stress ($f_{sv} \le f_y$) in the database specimens with lower concrete compressive strengths.

The strongest trend observed in Fig. 4 and Table 4 involves a/d. As with f'_c, it is reasoned that a/d affects the contribution of the transverse reinforcement. As a/d increases, inclined cracks cross greater amounts of reinforcement, and consequently, stress in the reinforcement decreases. In other words, more bars carry the force and stress in the bars is reduced.

Similar phenomena were considered by Ross and Naji[1] in the development of Eq. (6). While Eq. (6) was developed using a guess-and-check approach, the following section aims to create an equation for vertical reinforcement stress that is based on rigorous statistical formulation and analysis.

Evaluation of database using the least squares method

The method of least squares is a standard approach in regression analysis that minimizes the sum of the squares of the errors between a model and experimental data. In this case, the least squares method provides the best fit that minimizes the errors between nominal capacities V_{nb} and experimental capacities V_{exp} in 120 specimens of the database. The method is mathematically described as Eq. (8).

$$\text{Min} \sum_{j=1}^{120} \left(V_{nb}^j - V_{exp}^j \right)^2 \tag{8}$$

where

j = index for each of the 120 specimens

This definition is expanded by substituting Eq. (3) into Eq. (8) to give Eq. (9).

$$\text{Min} \sum_{j=1}^{120} \left(\frac{V_s^j x_s^j}{d^j \cot\theta^j} + \frac{T^j}{\cot\theta^j} + \frac{V_h^j d_h^j}{d^j} + \frac{H_h^j d_h^j}{d^j \cot\theta^j} - V_{exp}^j \right)^2 \tag{9}$$

As illustrated before, the strength ratio is inversely related to f'_c and directly related to a/d. It was also argued that both variables affect the stress in the transverse reinforcement. To account for these relationships, Eq. (10) includes f'_c in the numerator and a/d in the denominator of the first term. As already discussed, a/d is expressed as cot θ.

A factor α was also included in the first term for calibration purposes.

$$\text{Min}\sum_{j=1}^{120}\left(\frac{V_s^j x_s^j \alpha f_c^{'j}}{d^j \cot^2\theta^j}+\frac{T^j}{\cot\theta^j}+\frac{V_h^j d_h^j}{d^j}+\frac{H_h^j d_h^j}{d^j\cot\theta^j}-V_{exp}^j\right)^2 \quad (10)$$

The least squares method was used to minimize the sum of the squares of the errors between nominal capacities and experimental capacities by solving for α while also considering f_c' and a/d (expressed as $\cot\theta$) in the first term. In Eq. (10) T was calculated for each specimen using Eq. (4). By solving Eq. (10) for 120 specimens, α was determined to be 0.16; hence, the refined bond-loss capacity equation takes the form of Eq. (11).

$$V_{nb}=\frac{0.16V_s x_s f_c^{'}}{d\cot^2\theta}+\frac{T}{\cot\theta}+\frac{V_h d_h}{d}+\frac{H_h d_h}{d\cot\theta} \quad (11)$$

In the absence of harped strands, the equation can be written as Eq. (12).

$$V_{nb}=\frac{0.16V_s x_s f_c^{'}}{d\cot^2\theta}+\frac{T}{\cot\theta} \quad (12)$$

Recalling that compressive strength and shear span ratio affect stress in the transverse reinforcement, it is convenient to express Eq. (11) in the format of Eq. (13).

$$V_{nb}=\frac{V_{sb}x_s}{d\cot\theta}+\frac{T}{\cot\theta}+\frac{V_h d_h}{d}+\frac{H_h d_h}{d\cot\theta} \quad (13)$$

where

V_{sb} = force in transverse reinforcement coincident with bond-loss failure = $A_v f_{sb}$

f_{sb} = stress in transverse reinforcement coincident with bond-loss failure

$$f_{sb}=f_y\left(\frac{0.16f_c^{'}}{\cot\theta}\right)\le f_y \quad (14)$$

This approach relates transverse reinforcement stress to the shear span ratio (expressed as $\cot\theta$) and compressive strength of the concrete. When using Eq. (14), the concrete compressive strength must be provided in ksi units.

Validation of the refined model

Nominal bond-loss capacity, calculated using the refined model (Eq. [11]), was compared with the experimental capacity of each database specimen. As was done in Fig. 4, **Fig. 5** uses the strength ratio to compare the calculated and experimental results with six different variables. When performing the calculations, the lack of full development length was accounted for using Eq. (4).

Referring to Fig. 5, the strength ratios appear to be uniformly distributed around 1.0, indicating good agreement between the experimental data and the refined model. The average strength ratio was 0.98 with a coefficient of variation of 0.20. For comparison, the strength ratio and coefficient of variation for the first analysis were 1.47 and 0.51, respectively. Observations made from Fig. 5 are confirmed by results of a linear regression analysis (**Table 5**). Large P values (greater than 0.05) for all six variables indicate that the refined model provides a robust estimation over the range of all independent variables. To express it differently, the refined bond-loss capacity model (Eq. [11]) produces a uniform degree of accuracy and conservatism across the range of each considered variable.

The analysis presented in Table 4 indicated that the values from the original model are significantly related to a/d, f_c', d, and A_{ps}. However, after considering f_c' and a/d in the refined model, there is no longer a significant trend between the model results and d and A_{ps}. This is evident from the large (greater than 0.05) P values associated with d and A_{ps} (Table 5). Thus, the refinements based on a/d and f_c' were sufficient to create a robust model.

Comparison of model with AASHTO LRFD specifications

Strength ratios of all 120 specimens were calculated using both the refined model (Eq. [11]) and the AASHTO LRFD specifications (Eq. [2]). **Figure 6** compares them. In both cases the effects of reduced development of the tension tie were considered using Eq. (4). The AASHTO LRFD specifications end-region equilibrium model, which assumes yielding of the vertical reinforcement, resulted in calculated capacities that were 48% larger (unconservative) on average than the experimental capacities. The coefficient of variation of strength ratio for the AASHTO LRFD specifications was 0.51, approximately twice that of the refined model. Thus, the refined model produces results that are more accurate and have less scatter than the current AASHTO LRFD specifications. The refined model also has the added benefit of producing results that have relatively consistent levels of conservatism and accuracy for the ranges of the considered variables.

Example calculations

To aide in the application of the refined model, this section of the paper presents example calculations for an AASHTO Type III girder. **Table 6** summarizes the girder parameters, which are based on specimen G1 from a program by Ross et al.; specimen details and drawings are available in the Fall 2011 issue of *PCI Journal*.[7]

Calculation of force in harped strands

$F_h = A_{ph} f_{pe}(L_{dh}/L_t) < A_{ph} f_{pe}$

where

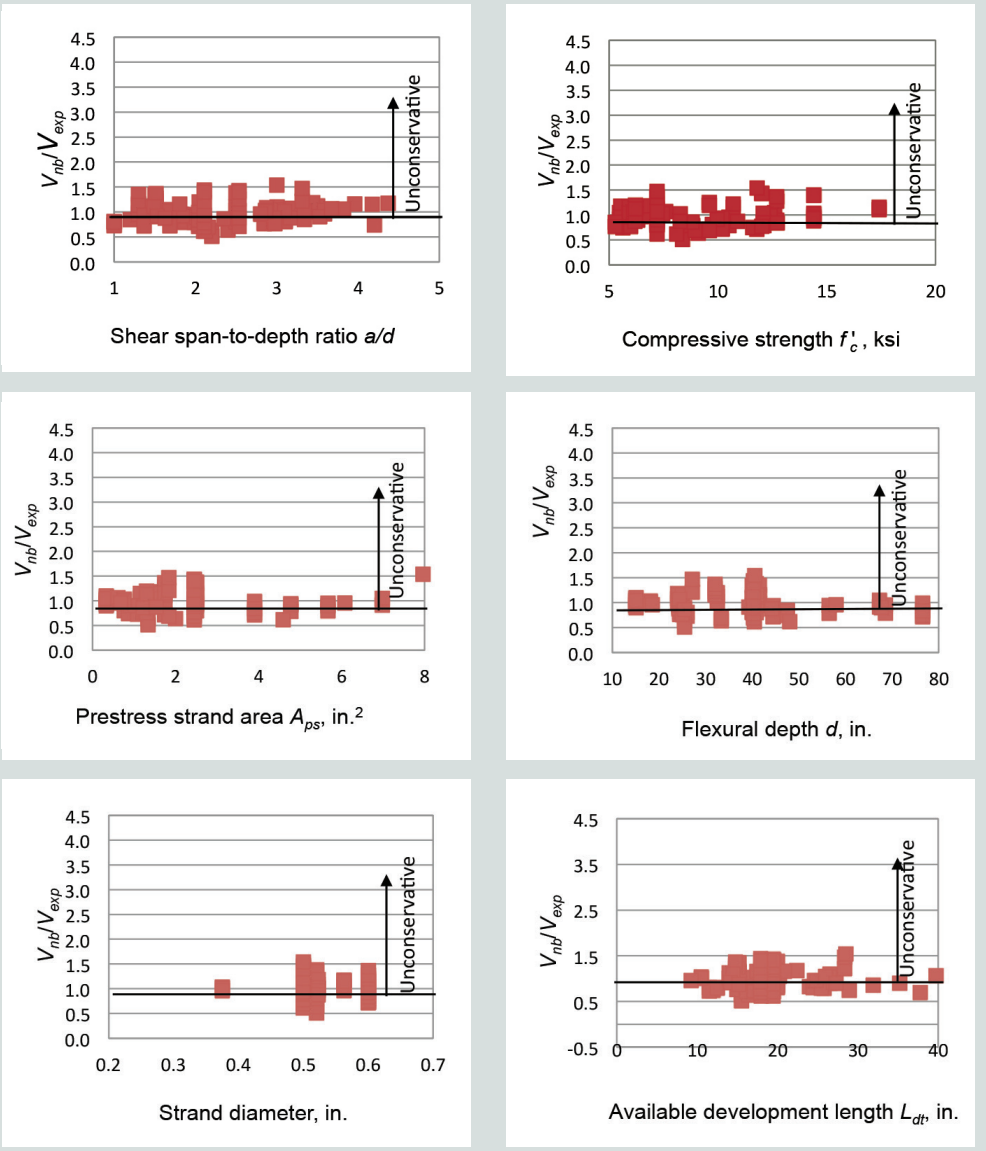

Figure 5. Strength ratios from refined model compared with specimen parameters. Note: V_{exp} = experimental bond capacity; V_{nb} = nominal bond capacity. 1 in. = 25.4 mm; 1 ksi = 6.895 MPa.

Table 5. Results of linear regression analysis for the refined model

Variables	Single regression analysis P value	Significant trend
Shear span–to–depth ratio *a/d*	0.217	No
Concrete compressive strength f'_c	0.192	No
Available embedment length of tension tie L_{dt}	0.651	No
Area of prestressing steel A_{ps}	0.683	No
Flexural depth of tension tie *d*	0.161	No
Strand diameter	0.726	No

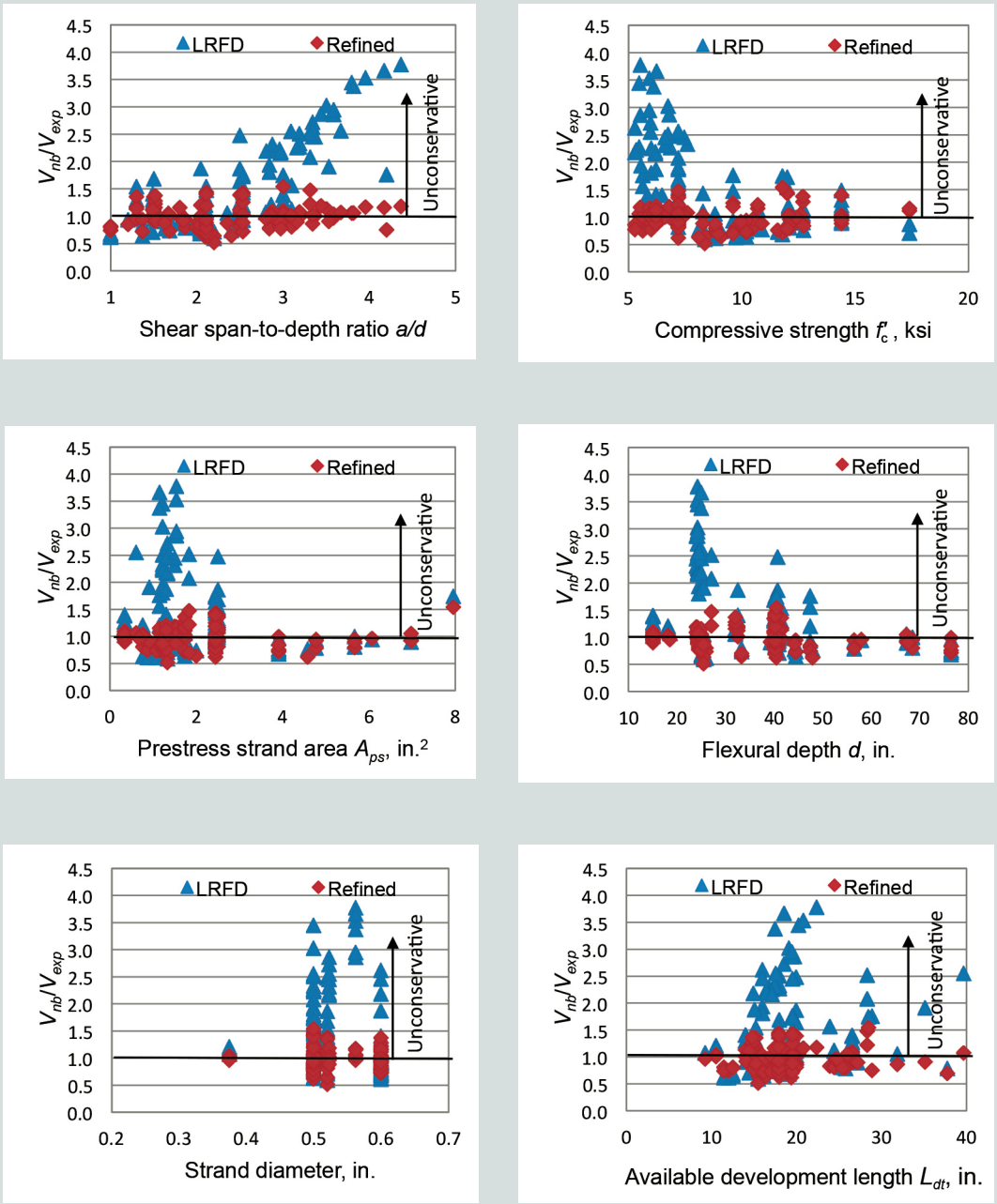

Figure 6. Comparison of strength ratios from 2014 *AASHTO LRFD Bridge Design Specifications* and refined models. Note: V_{exp} = experimental bond capacity; V_{nb} = nominal bond capacity. 1 in. = 25.4 mm; 1 ksi = 6.895 MPa.

F_h = total force in harped strands

A_{ph} = area of harped strands

$F_h = A_{ph} f_{pe}$ = 140 kip (623 kN)

$H_h = F_h(\cos \beta)$ = 139.5 kip (620.5 kN)

where

β = inclination angle of harped strands

V_h = $F_h(\sin \beta)$ = 11 kip (49 kN)

Calculation of tension tie force

$T = A_s f_y + A_{ps} f_{pe}(L_{dt}/L_t) < A_s f_y + A_{ps} f_{pe}$

$T = A_s f_y + A_{ps} f_{pe}(L_{dt}/L_t)$
$= (0.6)(60) + (1.152)(162)(15.4/30)$
$= 132$ kip (587 kN)

Table 6. Specimen parameters of girder G1

Item	Value	Notes
A_{ps}, in.^{2}	1.152	Eight ½ in. strands (value considers fully bonded straight strands that contribute to the tension tie)
f_{pe}, ksi	162	
A_s, in.^{2}	0.6	Three no. 4 bars
f'_c, ksi	5.63	Tested compressive strength
d, in.	47.5	
a, ft	4.75	Based on load and support geometry.
$a/d \approx \cot\theta$	1.2	
A_v, in.^{2}	4.88	Twelve no. 4 bars, eight no. 5 bars
x_s, in.	32.4	Specimen G1 had nonuniform distribution of transverse reinforcement. This value is the centroid of the transverse bars that cross the assumed crack.
f_y, ksi	60	
H, in.	52	Height of precast concrete girder and deck
X_{brg}, in.	8	Bearing distance
X_{oh}, in.	2	Overhang distance
$X_t = (H - d)(\cot\theta)$, in.	5.4	
$L_{dt} = X_{brg} + X_{oh} + X_t$, in.	15.4	
A_{ph}, in.^{2}	0.864	Six ½ in. strands
β, degrees	4.5	
L_{dh}, in.	45.3	
L_t, in.	30	Taken as 60 strands diameter per 2014 *AASHTO LRFD Bridge Design Specifications* section 5.11.4
d_h, in.	22.6	

Note: a = shear span; a/d = shear span-to-depth ratio; A_{ph} = area of harped strands; A_{ps} = area of prestressing steel; A_s = area of nonprestressing tension steel; A_v = area of vertical reinforcement crossing assumed crack plane; d = flexural depth of tension tie; d_h = depth of harped strands at crack interface; f'_c = concrete compressive strength; f_{pe} = effective stress in prestressing steel; f_y = specified yield strength of reinforcement bars; H = height of precast concrete girder and deck; L_{dh} = available embedment length of harped strand; L_{dt} = available embedment length of tension tie; L_t = required transfer length; x_s = horizontal distance to vertical steel centroid; X_{brg} = bearing distance; X_{oh} = overhang distance; X_t = horizontal distance between front of bearing and intersection of crack and tie; β = inclination angle of harped strands; θ = angle of inclination of diagonal compressive stresses. No. 4 = 13M; no. 5 = 16M; 1 in. = 25.4 mm; 1 ft = 0.305 m; 1 ksi = 6.895 MPa.

Calculation of force in transverse reinforcement (Eq. [14])

$$f_{sb} = f_y\left(\frac{0.16\sqrt{f'_c}}{\cot\theta}\right) = (60)\left[\frac{(0.16)(5.63)}{1.2}\right]$$

$$= 45 \text{ ksi } (310 \text{ MPa}) \le f_y$$

$$V_{sb} = A_v f_{sb} = (4.88)(45) = 220 \text{ kip } (980 \text{ kN})$$

Calculation of bond-loss capacity (Eq. [13])

$$V_{nb} = \frac{V_{sb}x_s}{d\cot\theta} + \frac{T}{\cot\theta} + \frac{V_h d_h}{d} + \frac{H_h d_h}{d\cot\theta} = \frac{(220)(32.4)}{(47.5)(1.2)} + \frac{132}{1.2} + \frac{(11)(22.6)}{47.5} + \frac{(139.5)(22.6)}{(47.5)(1.2)}$$

$$= 295 \text{ kip } (1310 \text{ kN})$$

The nominal bond-loss capacity ratio of the example is 0.85. In presenting this calculation example, an important limitation of the model should be mentioned. The model is based on bond loss due to cracking near the bearing (Fig. 1) but does not consider the embedment length of strands required to fully develop the flexural capacity of a given cross section. Development length must be separately checked to evaluate resistant to bending moments.

Conclusion

A previously published database of test specimens was expanded and then used to create a refined model for bond-loss resistance of pretensioned I-girders. The refined model was constructed using the least squares method and linear regression analysis. Salient conclusions are as follows:

- Results from regression analysis indicate that stress in the transverse reinforcement attendant at bond-loss failure is related to the shear span–to–depth ratio *a*/*d* and concrete compressive strength f'_c. With regard to shear span ratio, this result is attributed to the increased number of bars that are engaged as the ratio becomes larger: as more bars are engaged, the stress in the bars is decreased. With regard to concrete strength, this result is attributed to the effect of concrete on the peak capacity of the bond-loss mechanism. Lower concrete strength results in earlier failure of the compression zone, which is often the event that controls peak capacity in bond-loss failures; because the compression zone fails earlier, stress in the vertical reinforcement at failure is often less than yield.

- By considering the effects of concrete compressive strength and shear span–to–depth ratio, the refined model is a more accurate representation of bond-loss behavior. When results from the model are compared with values from specimens in the bond-loss database, the average strength ratio (calculated-to-experimental capacity) was 0.98 with a coefficient of variation of 0.2. In addition, large P values (greater than 0.05) in a regression analysis of the refined model indicate that the model provides a robust estimate over the range of each variable. In other words, the accuracy and conservatism of the refined model are consistent over the considered ranges of the independent variables.

- The refined model is a significant improvement in terms of accuracy and scatter compared with the current AASHTO LRFD specifications' end-region equilibrium model. The AASHTO LRFD specifications model resulted in calculated capacities that were 48% larger (unconservative) on average than the experimental capacities. The coefficient of variation of strength ratio for the AASHTO LRFD specifications model was 0.51, more than twice that of the refined model. The unconservative results from the AASHTO LRFD specifications model may be attributed to the assumption that vertical reinforcement always reaches yield stress.

Acknowledgments

The authors acknowledge the Glenn Department of Civil Engineering at Clemson University in Clemson, S.C., for supporting Behnam Naji during this research.

References

1. Ross, B. E., and B. Naji. 2014. "Model for Nominal Bond-Shear Capacity of Pretensioned Concrete Girders." *Transportation Research Record: Journal of the Transportation Research Board* 2406: 79–86.

2. AASHTO (American Association of State Highway and Transportation Officials). 2014. *AASHTO LRFD Bridge Design Specifications*. 7th ed., customary U.S. units. Washington, DC: AASHTO.

3. Deatherage, J. H., E. G. Burdette, and C. K. Chew. 1994. "Development Length and Lateral Spacing Requirements of Prestressing Strand for Prestressed Concrete Bridge Girders." *PCI Journal* 39 (1): 70–83.

4. Shahway, M. A., and B. Batchelor. 1996. "Shear Behavior of Full-Scale Prestressed Concrete Girders: Comparison Between AASHTO Specifications and LRFD Code." *PCI Journal* 41 (3): 48–62.

5. Abdalla, O. A., J. A. Ramirez, and R. H. Lee. 1993. *Strand Debonding in Pretensioned Beams-Precast Prestressed Concrete Bridges with Debonded Strands*. Report FAWA/INDOT/JHRP-92-25. Indianapolis, IN: Indiana Department of Transportation.

6. Naji, B., B. E. Ross, and R. W. Floyd. 2017. "Characterization of Bond-Loss Failures in Pretensioned Concrete Girders." *Journal of Bridge Engineering* 22 (4). https://doi.org/10.1061/(ASCE)BE.1943-5592.0001025.

7. Ross, B. E., M. H. Ansley, and H. R. Hamilton III. 2011. "Load Testing of 30-year-old AASHTO Type III Highway Bridge Girders." *PCI Journal* 56 (4): 152–163.

8. Garber, D. B., J. M. Gallardo, D. J. Deschenes, and O. Bayrak. 2016. "Nontraditional Shear Failures in Bulb-T Prestressed Concrete Bridge Girders." *Journal of Bridge Engineering* 21 (7). https://doi.org/10.1061/(ASCE)BE.1943-5592.0000890.

9. Ross, B. E., H. R. Hamilton, and G. R. Consolazio. 2015. "Experimental Study of End Region Detailing and Shear Behavior of Concrete I-Girders." *Journal of Bridge Engineering* 20 (6). https://doi.org/10.1061/(ASCE)BE.1943-5592.0000676.

10. Ross, B. E., H. R. Hamilton, and G. R. Consolazio. 2013. *End Region Detailing of Pretensioned Concrete Bridge Girders*. Report BDK75 977-05. Tallahassee, FL: Florida Department of Transportation.

11. Ross, B. E., H. R. Hamilton, and G. R. Consolazio. 2011. "Experimental and Analytical Evaluations of Confinement Reinforcement in Pretensioned Concrete Beams." *Transportation Research Record: Journal of the Transportation Research Board* 2251: 59–67.

12. Kaufman, M. K., and J. A. Ramirez. 1988. "Re-evaluation of the Ultimate Shear Behavior of High-Strength Concrete Prestressed I-Beams." *ACI Structural Journal* 85 (3): 295–303.

13. Barnes, R. W., N. H. Burns, and M. E. Kreger. 1999. *Development Length of 0.6-Inch Prestressing Strand in Standard I-Shaped Pretensioned Concrete Beams*. Report FHWA/TX-02/1388-1. Austin, TX: Texas Department of Transportation.

14. Hawkins, N. M., and D. A. Kuchma. 2007. *Application of LRFD Bridge Design Specifications to High-Strength Structural Concrete: Shear Provisions*. National Cooperative Highway Research Program report 579. Washington, DC: Transportation Research Board.

15. Ma, Z., M. K. Tadros, and M. Baishya. 2000. "Shear Behavior of Pretensioned High-Strength Concrete Bridge I-Girders." *ACI Structural Journal* 97 (1): 185–192.

16. Maruyama, K., and S. H. Rizkalla. 1988. "Shear Design Consideration for Pretensioned Prestressed Beams." *ACI Structural Journal* 85 (5): 492–498.

17. Alshegeir, A., and J. A. Ramirez. 1992. "Strut-Tie Approach in Pretensioned Deep Beams." *ACI Structural Journal* 89 (3): 296–304.

18. Labonte, T., and H. R. Hamilton. 2005. *Self-Consolidating Concrete (SCC) Structural Investigation*. Report BD545-RPWO 21. Tallahassee, FL: Florida Department of Transportation.

19. Hartmann, D. L., J. E. Breen, and M. E. Kreger. 1988. *Shear Capacity of High Strength Prestressed Concrete Girders*. Report FHWA/TX-88+381-2. Austin, TX: Texas Department of Transportation.

20. Kahn, L. F., J. C. Dill, and C. G. Reutlinger. 2002. "Transfer and Development Length of 15-mm Strand in High Performance Concrete Girders." *Journal of Structural Engineering* 128 (7): 913–921. https://doi.org/10.1061/(ASCE)0733-9445(2002)128:7(913).

21. Meyer, K. F., L. F. Kahn, J. S. Lai, and K. E. Kurtis. 2002. *Behavior of High-Strength/High-Performance Lightweight Concrete Prestressed Girders*. Report 2004. Atlanta, GA: Georgia Department of Transportation.

22. Jongpitaksseel, N. 2003. "Behavior of End Zone of Precast/Pretensioned Concrete Bridge Girders." PhD diss., University of Nebraska, Lincoln, NE.

23. Raymond, K. K., R. N. Bruce, and J. J. Roller. 2005. "Shear Behavior of HPC Bulb-Tee Girders." *ACI Special Publication* 228: 705–722.

24. Tawfiq, K. S., 1995. *Cracking and Shear Capacity of High Strength Concrete Bridge Girders*. Report FL/DOT/RMC/612(1)-4269. Tallahassee, FL: Florida Department of Transportation.

25. Tawfiq, K. S., 1996. *Cracking and Shear Capacity of High Strength Concrete Bridge Girders under Fatigue Loading*. Report FL-DOT RMC. Tallahassee, FL: Florida Department of Transportation.

26. Hines, W. W., D. C. Montgomery, D. M. Goldsman, and C. M. Borror. 2003. *Probability and Statistics in Engineering*. New York, NY: John Wiley and Sons.

27. Ramirez-Garcia, A. T., R. W. Floyd, W. M. Hale, and J. R. Martí-Vargas. 2016. "Effect of Concrete Compressive Strength on Transfer Length." *Structures* 5: 131–140.

Notation

a = shear span

a/d = shear span–to–depth ratio

A_{ph} = area of harped strands

A_{ps} = area of prestressing steel contributing to the tension tie

A_s = area of nonprestressing tension steel

A_v = area of vertical reinforcement crossing assumed crack plane

b_w = web width

C = force in compression zone

d = flexural depth of tension tie

d_h = depth of harped strands at crack interface

d_v = effective shear depth

f_1 = empirical factor

f_2 = empirical factor

f'_c = concrete compressive strength

f_{pe} = effective stress in prestressing steel

f_{ps} = average stress in prestressing steel coincident with V_u

f_{psb} = stress in prestressing strand coincident with bond-loss failure

f_{sb} = stress in vertical reinforcement coincident with bond-loss failure

f_{sv} = stress in vertical reinforcement

f_y = specified yield strength of reinforcement bars

F_h = total force in harped strands

H = height of precast concrete girder and deck

H_h = horizontal force in harped strand

L_{dh} = available embedment length of harped strand

L_{dt} = available embedment length of tension tie

L_t = required transfer length

T = longitudinal tie force in flexural reinforcement

V_a = force along crack interface

V_{exp} = experimental bond capacity

V_h = vertical force in harped strand

V_{nb} = nominal bond capacity

V_p = component of prestressing in direction of the shear force

V_s = resistance provided by the vertical reinforcement

V_{sb} = force in vertical reinforcement coincident with bond-loss failure

V_u = factored shear force

x_s = horizontal distance to vertical steel centroid

X_{brg} = bearing distance

X_{oh} = overhang distance

X_t = horizontal distance between front of bearing and intersection of crack and tie

α = calibration factor

β = inclination angle of harped strands

θ = angle of inclination of diagonal compressive stresses

κ_{sv} = empirical factor

ρ_{sv} = shear reinforcement ratio

ϕ_v = resistance factor for shear

About the authors

Behnam Naji, PhD, works for the product and process development department at Tindall Corp. in Atlanta, Ga. He earned his PhD in civil engineering at Clemson University in Clemson, S.C.

Brandon E. Ross, PhD, PE, is an assistant professor in the Glenn Department of Civil Engineering at Clemson University.

Amin Khademi, PhD, is an assistant professor in the Industrial Engineering department at Clemson University.

Abstract

Bond-loss failures have been observed in load tests of precast, pretensioned concrete I-girders. This type of failure is associated with shear cracking near the support that interrupts anchorage of the strands, leading to loss of bond and slipping of the strands relative to the concrete. This paper presents a database of bond-loss failures that are documented in the research literature and uses the database to create a bond-loss failure model. The database and model are expansions and refinements of the authors' previous work on the subject. The refined model is created through linear regression and least squares analyses and is demonstrated to have superior accuracy compared with the end-region model in section 5.8.3.5-2 of the American Association of State Highway and Transportation Officials' 2014 *AASHTO LRFD Bridge Design Specifications*. One of the key insights accounted for in the refined model is that stress in transverse reinforcement attendant with bond-loss failure is often less than yield stress.

Keywords

Bond-loss failure, database, end region, girder, I-girder, least squares method, load test, refined model, regression analysis.

Review policy

This paper was reviewed in accordance with the Precast/Prestressed Concrete Institute's peer-review process.

Reader comments

Please address reader comments to journal@pci.org or Precast/Prestressed Concrete Institute, c/o *PCI Journal*, 200 W. Adams St., Suite 2100, Chicago, IL 60606.